

Correlated Defects, Metal-Insulator Transition, and Magnetic Order in Ferromagnetic Semiconductors

C. Timm,* F. Schäfer, and F. von Oppen

Institut für Theoretische Physik, Freie Universität Berlin, Arnimallee 14, D-14195 Berlin, Germany

(Received 22 January 2002; published 5 September 2002)

The effect of disorder on transport and magnetization in ferromagnetic III-V semiconductors, in particular (Ga,Mn)As, is studied theoretically. We show that Coulomb-induced correlations of the defect positions are crucial for the transport and magnetic properties of these highly compensated materials. We employ Monte Carlo simulations to obtain the correlated defect distributions. Exact diagonalization gives reasonable results for the spectrum of valence-band holes and the metal-insulator transition only for correlated disorder. Finally, we show that the mean-field magnetization also depends crucially on defect correlations.

DOI: 10.1103/PhysRevLett.89.137201

PACS numbers: 75.50.Pp, 71.30.+h, 72.20.Ee

Introduction.—Recently, there has been substantial interest in diluted ferromagnetic III-V semiconductors due to observations of relatively high Curie temperatures [1–3]. This makes these materials promising for applications as well as interesting from the physics point of view. They could allow the incorporation of ferromagnetic elements into semiconductor devices and, thus, the integration of processing and magnetic storage on a single chip. To be specific, we consider here manganese-doped GaAs. The properties of this material rely on the dual role played by the Mn impurities: They carry a local spin due to their half-filled d shell and dope the system with holes, which mediate a ferromagnetic indirect exchange interaction between the spins. Furthermore, the materials are highly compensated, presumably due to antisite defects (As substituted for Ga) [4], which drives them towards a metal-insulator transition (MIT). It is clearly important to understand the interplay between transport properties, magnetic ordering, and the defect configuration. In this Letter, we show that *correlated* defects are required for a description consistent with experiments.

There is a growing body of theoretical work on (Ga,Mn)As [5]. Most approaches either start from the heavily doped regime [6–12] or from the weak-doping limit [13]. In the case of heavy doping [6–12], one considers valence-band holes moving in the disorder potential of the defects. For large hole concentration, the Fermi energy E_F lies deep in the valence band compared to the Coulomb-potential fluctuations, and the latter are neglected. On the other hand, for light doping [13], the local impurity states overlap only weakly, forming an impurity band. This model is problematic since for the typical doping range the impurity band would be much broader than the energy gap [14]. Both approaches have in common that the effect of antisites on the disorder and correlations of defects are neglected.

The outline of the remainder of this Letter is as follows. First, we discuss the configuration of Mn impurities and antisite defects with the help of Monte Carlo simu-

lations and obtain the disorder potential and its spatial correlations. Then, we derive the spectrum and localization properties of holes in this potential and discuss the MIT. Finally, we calculate the polarizations of Mn and hole spins within a self-consistent mean-field theory.

Defect configurations.—In the theory of doped semiconductors, one often assumes the dopants to be randomly distributed [5,15]. However, the present system is highly compensated. This leads to defects of either charge being present (relative to Ga, Mn impurities have charge $-e$ while antisites carry $+2e$) and to a low density of carriers, which only weakly screen the Coulomb interaction between the charged defects [15]. In the resulting *Coulomb plasma*, the defect positions are expected to be highly correlated. We study here the limiting case where the defects come into thermal equilibrium during growth [16]. This is motivated by experiments [4] suggesting that defects diffuse rapidly at 250 °C, which is a typical growth and annealing temperature for (Ga,Mn)As grown by molecular beam epitaxy. The resulting configuration is assumed to be quenched at low temperatures.

To find typical defect configurations close to equilibrium, we perform Monte Carlo simulations for the classical Coulomb system of Mn impurities and antisites on the Ga sublattice with the Hamiltonian $H = 1/2 \sum_{i,j} q_i q_j / (\epsilon r_{ij}) e^{-r_{ij}/r_{scr}}$, where q_i are the defect charges, r_{ij} is their separation, and $\epsilon \cong 11$. The screening length r_{scr} is obtained from nonlinear screening theory [15]. r_{scr} is much larger than the nearest-neighbor separation of Ga sites for realistic parameters so that it hardly affects the small-scale defect correlations relevant here. We employ the Metropolis algorithm at 250 °C for systems of $20 \times 20 \times 20$ conventional cubic unit cells with periodic boundary conditions, unless stated otherwise.

A typical result for Mn concentration $x = 0.05$ and $p = 0.3$ holes per Mn, as suggested by experiments [1], is shown in Fig. 1. The concentration of antisites is obtained from x and p under the assumption of charge neutrality.

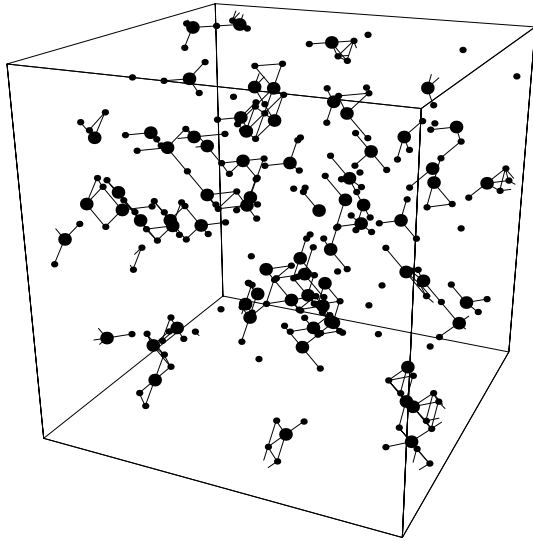


FIG. 1. Typical equilibrium configuration at 250 °C for 5% Mn doping and 0.3 holes per Mn. Only the defects are shown, large (small) circles denote antisite (Mn) defects. Defects at nearest-neighbor Ga sites are connected by a bond. For clarity, we show only $10 \times 10 \times 10$ conventional unit cells.

Most of the defects have formed clusters. This leads to screening of the disorder potential by the defects, as can be seen from the potential correlation function $D(r) \equiv \langle V(\mathbf{r})V(\mathbf{r}') \rangle_{|\mathbf{r}-\mathbf{r}'|=r} - \langle V \rangle^2$ plotted in Fig. 2 for $x = 0.05$ and $p = 0.3$. Note that $\Delta V \equiv \sqrt{D(0)}$ is the width of the distribution of $V(\mathbf{r})$. For correlated defects, $D(r)$ and thus ΔV are strongly reduced and the Coulomb potential is screened on the much shorter length scale r_{ion} , which is of the order of the nearest-neighbor Ga site separation [17]. (This ionic screening is possible due only to the presence of defects of either charge. Thus it does not take place, e.g., in ferromagnetic II-VI semiconductors since Mn is isovalent in these materials.) Importantly, however, $\Delta V \approx 0.284$ eV is still *not* small compared to the Fermi energy $|E_F| \approx 0.329$ eV.

Recent high resolution x-ray diffraction [18] as well as resistivity and magnetization measurements [4] support the formation of small clusters. The more direct determination of the local structure around Mn dopants by extended x-ray-absorption fine structure [19] does not give direct information on the abundance of specific elements around the Mn. However, the observed loss of order around Mn is certainly consistent with cluster formation. Finally, we show in the following that experimental results for the band gap, transport, and the magnetization [1,20] strongly support the clustering.

Hole states.—To find the spectrum and localization properties of valence-band holes moving in the disorder potential $V(\mathbf{r})$, we start from the Hamiltonian $H = -\sum_i (\hbar^2/2m^*) \nabla_i^2 + V(\mathbf{r}_i)$, where we use the envelope function and parabolic-band approximations [21]. The calculations are done for spinless holes, which is justified

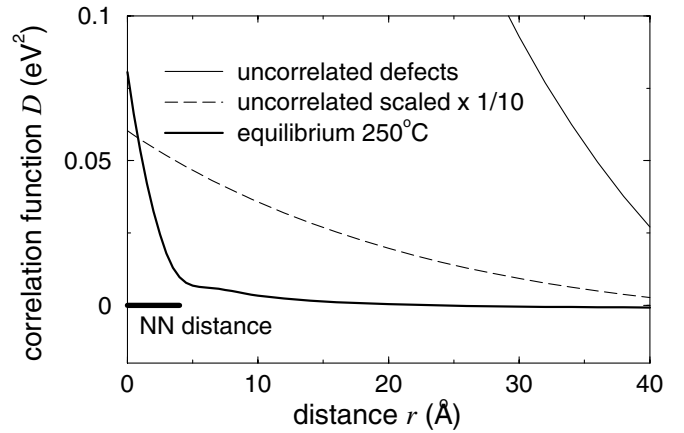


FIG. 2. Potential correlation function $D(r)$ for 5% Mn and 0.3 holes per Mn, both for uncorrelated defects and for equilibrium at the growth temperature. The nearest-neighbor Ga site separation of 3.99 Å is also indicated.

since the additional disorder introduced by the exchange interaction with the Mn spins is much smaller than ΔV .

The Hamiltonian is solved by exact diagonalization in a plane-wave basis of $13^3 = 2197$ states [22], giving the energy spectrum and normalized eigenfunctions. The Fermi energy E_F is obtained from the hole concentration px . We also obtain the inverse participation ratio $\text{IPR}(n) = 1/\sum_{\mathbf{r}} |\psi_n(\mathbf{r})|^4$ of the states $\psi_n(\mathbf{r})$. The IPR allows one to estimate the position of the mobility edge, since it is of the order of the volume for extended states but is essentially independent of system size for localized states. Figure 3 shows a comparison of the IPR as a function of energy for uncorrelated defects and for the equilibrium configuration obtained above for 5% Mn and 0.3 holes per Mn. The valence-band edge is strongly smeared out by uncorrelated defects so that the energy gap is completely filled, which is not observed experimentally, whereas correlated defects lead only to a small

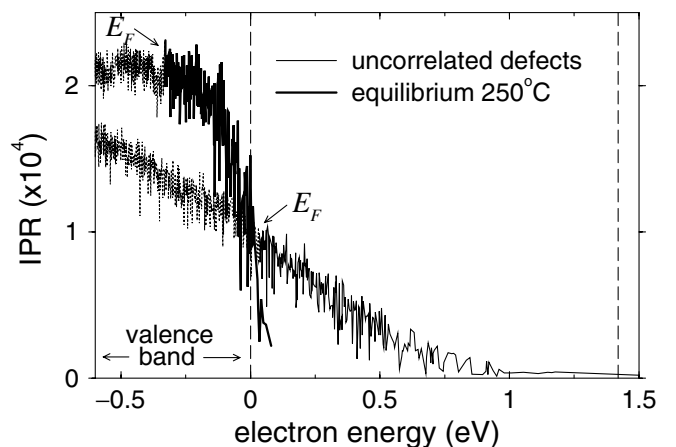


FIG. 3. IPR as a function of energy at the valence-band edge for 5% Mn and 0.3 holes per Mn. The thin (heavy) solid line denotes empty states for uncorrelated (correlated) defects; the dotted lines denote occupied states.

tail in the gap. We have also studied the dependence of the IPR on system size L^3 over the limited feasible range in L , finding that $\text{IPR}(n) \propto L^3$ for the flat part of the curve, signifying extended states, whereas the IPR is independent of L for states sufficiently far in the tail, which are thus localized. Hence, the mobility edge lies on the slope of the curve. The states are much more localized for uncorrelated defects, due to the larger disorder potential, whereas for correlated defects the states close to E_F are clearly extended. Thus, the spectrum and the localization properties agree with experiments [1] only for correlated defects.

In Fig. 4 we show the IPR as a function of energy for correlated defects at various Mn dopings and hole concentrations. The hole concentration for given Mn doping was chosen in accordance with experiments [1,23]. The spectrum and the IPR change little with Mn doping, since the potential screened by the defects on the length scale r_{ion} is much less affected by a change of concentration than the bare Coulomb potential.

The dominant effect comes from the hole concentration. Our result for the scaling of the IPR suggests that for 5% and 3% Mn the states at E_F are extended and we expect metallic behavior. For 1% Mn E_F is close to the mobility edge, while for 0.5% Mn the states at E_F are localized. From this we estimate the MIT to take place at a Mn concentration of the order of 1%. This result is in reasonable agreement with experiments [1]. For comparison, uncorrelated defects would lead to an MIT at about 5% Mn; see Fig. 3.

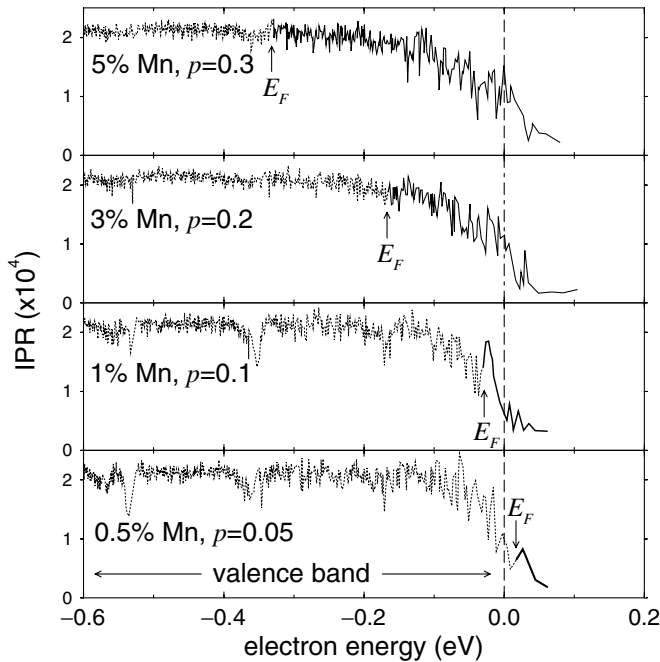


FIG. 4. IPR as a function of energy at the valence-band edge for various Mn dopings and hole concentrations p per Mn taken from experiment [1,23].

Magnetization.—Finally, we discuss the spontaneous magnetization and its dependence of the defect configuration. The exchange interaction between hole and Mn spins is described by the Hamiltonian $H = -\sum_i (\hbar^2/2m^*) \nabla_i^2 + V(\mathbf{r}_i) - J_{\text{pd}} \sum_{i,l} \mathbf{s}_i \cdot \mathbf{S}_l \delta(\mathbf{r}_i - \mathbf{R}_l)$, where $V(\mathbf{r})$ is the disorder potential obtained above, $J_{\text{pd}} \approx -45 \text{ eV \AA}^3$ is the exchange integral [9,24,25], \mathbf{s}_i and \mathbf{S}_l are the hole and Mn spin operators, respectively, and \mathbf{R}_l are the Mn impurity positions. In second quantized form, the Hamiltonian reads

$$H = \sum_{n\sigma} c_{n\sigma}^\dagger \epsilon_n c_{n\sigma} - J_{\text{pd}} \sum_{n\sigma, n'\sigma'} \sum_l c_{n\sigma}^\dagger \psi_n^*(\mathbf{R}_l) \frac{\boldsymbol{\tau}_{\sigma\sigma'}}{2} \cdot \mathbf{S}_l \psi_{n'}(\mathbf{R}_l) c_{n'\sigma'}, \quad (1)$$

where ϵ_n are the eigenenergies obtained in the absence of exchange as discussed above, $\psi_n(\mathbf{r})$ are the corresponding eigenfunctions, and $\boldsymbol{\tau}$ is the vector of Pauli matrices. The exchange interaction is decoupled at the mean-field level, introducing the averaged Mn spin polarizations $\mathbf{M}_l \equiv \langle \mathbf{S}_l \rangle$ and hole spin polarizations at the Mn sites, $\mathbf{m}_l \equiv \langle \sum_{n\sigma, n'\sigma'} c_{n\sigma}^\dagger \psi_n^*(\mathbf{R}_l) (\boldsymbol{\tau}_{\sigma\sigma'}/2) \psi_{n'}(\mathbf{R}_l) c_{n'\sigma'} \rangle$. We do *not* perform a spatial average; i.e., the disorder is retained. The hole and Mn sectors can now be diagonalized separately, \mathbf{M}_l and \mathbf{m}_l are calculated, and the procedure is iterated. This self-consistent mean-field theory is similar to the one employed by Berciu and Bhatt [13]. The main difference is that we start from realistic hole states for the disorder potential.

Figure 5(a) shows the Mn and hole spin polarizations for $x = 0.05$ and $p = 0.3$. Also shown are the polarizations obtained neglecting disorder by using plane waves for the hole states and the virtual crystal approximation (VCA) for the Mn spins [5,7,21]. We see that disorder strongly enhances T_c [13]. This increase is easily understood: T_c is determined by the indirect exchange interaction of nearest-neighbor Mn pairs, which is inversely proportional to the separation [6–8]. Without disorder, the typical distance is $r_{\text{vca}} \sim n_{\text{Mn}}^{-1/3}$, where n_{Mn} is the density of Mn impurities. For $x = 0.05$, $r_{\text{vca}} \sim 9.67 \text{ \AA}$. On the other hand, with disorder the nearest-neighbor separation on the Ga sublattice is $r_{\text{dis}} = 3.99 \text{ \AA}$. Therefore, the indirect exchange, and thus T_c , is larger by a factor of order $r_{\text{vca}}/r_{\text{dis}} \sim 2.4$ in the disordered case.

For *correlated* defects the polarization curve looks more “mean-field-like,” in qualitative agreement with experiments [1,10,20]. This can be explained by the extended nature of the relevant hole states for correlated defects, which leads to a long-range indirect exchange interaction. Thus the effective field seen by a Mn spin is averaged over many other Mn spins and the spatial fluctuations of this effective field are small. On the other hand, for *uncorrelated* defects the holes are partly localized, the indirect exchange is of shorter range, and the fluctuations are larger. We believe that this leads to the smeared out magnetization curve. It is clearly

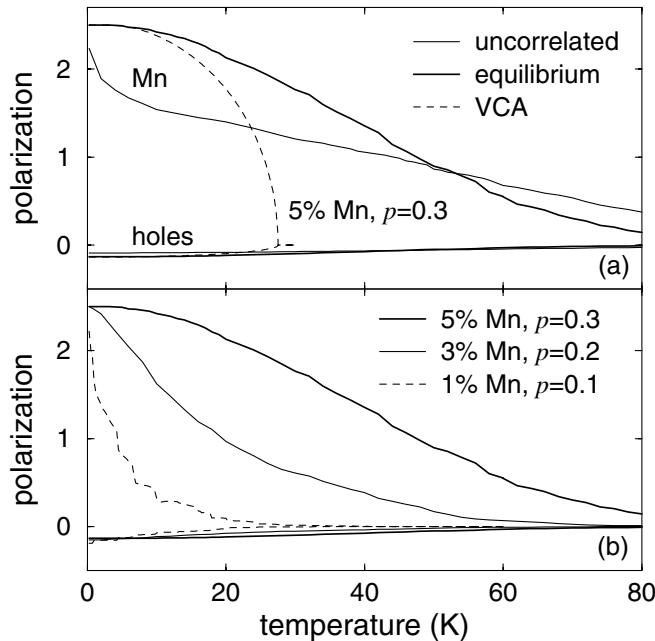


FIG. 5. (a) Magnetization as a function of temperature for 5% Mn and 0.3 holes per Mn, both for uncorrelated and correlated defects. The results denoted by “VCA” neglect disorder. (b) Magnetization for various Mn and hole concentrations (with correlated defects).

important to study the effect of fluctuations on the magnetization. We expect fluctuations to reduce T_c in particular for the uncorrelated case. Figure 5(b) shows that T_c is reduced for smaller Mn and hole concentrations and that the typical temperature scale is approximately proportional to x , in accordance with experiments [1]. Note also that in all cases the holes are only partially polarized.

To conclude, we have obtained typical defect configurations in (Ga,Mn)As and studied the effect of the resulting disorder potential on the valence-band holes. The strong Coulomb interactions of charged defects leads to the formation of defect clusters during growth. The previously neglected antisite defects are crucial for this effect. We have shown that such a correlated defect distribution is required to understand the hole spectrum, the metal-insulator transition, and the shape of the magnetization curves. Our results should also help to clarify why the properties of ferromagnetic semiconductors depend so strongly on details of the growth process.

We profited from discussions with P. J. Jensen, J. König, J. Schliemann, and, in particular, M. E. Raikh, who emphasized to us the importance of compensation.

Note added.—Recently, Yang and MacDonald [26] have studied the effect of the hole-hole interaction, assuming a random distribution of Mn dopants and antisites.

*Electronic address: timm@physik.fu-berlin.de

- [1] H. Ohno, *Science* **281**, 951 (1998); *J. Magn. Magn. Mater.* **200**, 110 (1999); H. Ohno and F. Matsukura, *Solid State Commun.* **117**, 179 (2001).
- [2] H. Ohno *et al.*, *Appl. Phys. Lett.* **69**, 363 (1996); F. Matsukura *et al.*, *Phys. Rev. B* **57**, R2037 (1998).
- [3] M. L. Reed *et al.*, *Appl. Phys. Lett.* **79**, 3473 (2001).
- [4] S. J. Potashnik *et al.*, *Appl. Phys. Lett.* **79**, 1495 (2001); see also R. C. Lutz *et al.*, *Physica (Amsterdam)* **273B–274B**, 722 (1999).
- [5] For a review, see J. König *et al.*, in “Electronic Structure and Magnetism of Complex Materials,” edited by D. J. Singh and D. A. Papaconstantopoulos (Springer, Berlin, 2002) (to be published), cond-mat/0111314.
- [6] T. Dietl, A. Haury, and Y. Merle d’Aubigné, *Phys. Rev. B* **55**, R3347 (1997); T. Dietl *et al.*, *Science* **287**, 1019 (2000).
- [7] T. Jungwirth *et al.*, *Phys. Rev. B* **59**, 9818 (1999).
- [8] J. König, H.-H. Lin, and A. H. MacDonald, *Phys. Rev. Lett.* **84**, 5628 (2000); J. König, T. Jungwirth, and A. H. MacDonald, *Phys. Rev. B* **64**, 184423 (2001).
- [9] M. Abolfath *et al.*, *Phys. Rev. B* **63**, 054418 (2001).
- [10] T. Dietl, H. Ohno, and F. Matsukura, *Phys. Rev. B* **63**, 195205 (2001).
- [11] A. Chattopadhyay, S. Das Sarma, and A. J. Millis, *Phys. Rev. Lett.* **87**, 227202 (2001).
- [12] J. Schliemann and A. H. MacDonald, *Phys. Rev. Lett.* **88**, 137201 (2002).
- [13] M. Berciu and R. N. Bhatt, *Phys. Rev. Lett.* **87**, 107203 (2001); cond-mat/0111045.
- [14] C. Timm, F. Schäfer, and F. von Oppen, *Phys. Rev. Lett.* (to be published), cond-mat/0111504; M. Berciu and R. N. Bhatt, *Phys. Rev. Lett.* (to be published), cond-mat/0112165.
- [15] B. I. Shklovskii and A. L. Efros, *Electronic Properties of Doped Semiconductors*, Solid-State Sciences Vol. 45 (Springer, Berlin, 1984).
- [16] L. V. Keldysh and G. P. Proshko, *Fiz. Tverd. Tela (Leningrad)* **5**, 3378 (1963) [*Sov. Phys. Solid State* **6**, 1093 (1964)].
- [17] The electronic screening length r_{scr} decreases for reduced disorder potential. However, r_{ion} is always the smaller, and thus relevant, length scale.
- [18] G. M. Schott, W. Faschinger, and L. W. Molenkamp, *Appl. Phys. Lett.* **79**, 1807 (2001).
- [19] R. Shioda *et al.*, *Phys. Rev. B* **58**, 1100 (1998).
- [20] B. Beschoten *et al.*, *Phys. Rev. Lett.* **83**, 3073 (1999).
- [21] For material-specific calculations, the detailed band structure should be taken into account [9,10]. This should not change the qualitative results but is known to increase the mean-field T_c [10].
- [22] We have checked that the results do not change significantly if the number of plane waves is increased.
- [23] F. Matsukura *et al.*, *Phys. Rev. B* **57**, R2037 (1998).
- [24] J. Okabayashi *et al.*, *Phys. Rev. B* **58**, R4211 (1998).
- [25] A. K. Bhattacharjee and C. Benoit à la Guillaume, *Solid State Commun.* **113**, 17 (2000).
- [26] S.-R. E. Yang and A. H. MacDonald, *Phys. Rev. Lett.* (to be published), cond-mat/0202021.